Zeitschrift: Schweizerische mineralogische und petrographische Mitteilungen = Bulletin suisse de minéralogie et pétrographie

Band: 83 (2003)

Heft: 3

Artikel: Chronological constraints of late- and post-orogenic emplacement of lamprophyre dykes in the southeastern Bohemian Massif, Austria

Autor: Neubauer, Franz / Dallmeyer, R. David / Fritz, Harald

DOI: https://doi.org/10.5169/seals-63152

Schweizerische Mineralogische und Petrographische Mitteilungen 83, 317–330, 2003

Chronological constraints of late- and post-orogenic emplacement of lamprophyre dykes in the southeastern Bohemian Massif, Austria

Franz Neubauer[1], *R. David Dallmeyer*[2] and *Harald Fritz*[3]

Abstract

Southeastern sectors of the Bohemian Massif are locally transected by two generations of lamprophyric dykes which post-date internal Variscan deformation of the variably metamorphosed constituent nappe units. Dykes of the first generation trend ESE, are locally weakly foliated and have been variably affected by low grade metamorphism. This generation is interpreted to have been emplaced during final WNW–ESE shortening of both external and internal nappe complexes. A 323 ± 3 Ma $^{40}Ar/^{39}Ar$ biotite plateau age from a representative unmetamorphosed dyke of the first generation is interpreted to reflect cooling after magmatic crystallisation. Second generation dykes are unfoliated and unmetamorphosed. These follow a major NNE-trend, and were emplaced into all nappe complexes of internal sectors of the orogen after regional Variscan deformation and metamorphism. Three biotite concentrates from the younger dykes record $^{40}Ar/^{39}Ar$ plateau ages of 315–306 Ma. Chemical compositions of second generation dykes vary from monzogabbroic, potassic mafic to trachyandesitic of a high-K series. They are interpreted to have originated from a crust-contaminated mantle source which likely resulted from post-collisional remelting of subducted lithosphere. Emplacement was related to late stage orogenic extension which allowed ascent of magmas generated by post-collisional remelting of subducted lithosphere or within the asthenosphere following lithospheric break-off. The new data constrain an interval of some 10–20 My between Variscan plate collision and subsequent late-stage extension.

Keywords: Variscides, slab break-off, extension, compression, orogeny.

1. Introduction

Dyke systems can allow resolution of regional stress conditions maintained in consolidated continental crust (e. g., Price and Cosgrove, 1990; Suppe, 1985). Their emplacement may also provide important brackets for times of deformation. Emplacement of mafic dykes is controlled by several parameters including the high density and low viscosity of such magmas, and the yield strength of the lithosphere (Emerman and Marrett, 1990; Sparks, 1992; Clemens and Mawer, 1992). Dykes are generally assumed to be emplaced within extensional fissures with boundaries parallel to the maximum principal stress axis (e. g., Suppe, 1985), with hydraulic fracturing leading to fracture opening where the tensile strength of the rock is exceeded (e. g., Price and Cosgrove, 1990; Sparks, 1992). The present study was initiated to document the significance of dyke systems in the evaluation of effective stresses during syn- and post-orogenic dyke emplacement in the southeastern Bohemian Massif. Because ascent of the magmas was associated with regional tensional failure of the lithosphere, dykes can be used to bracket internal deformation of the metamorphic nappe complex and constrain the post-Variscan cooling and tectonic erosion that postdates crustal shortening.

2. Structural and temporal framework

The southeastern Bohemian Massif comprises the external Moravo-Silesian and the internal Moldanubian units (Fig. 1). The Moravo-Silesian unit includes a late Proterozoic (Cadomian) basement, a Silurian to Early Carboniferous platform, and slope sequences and Visean flysch deposits (for reviews, see Fuchs and Matura, 1976; Franke, 1989; Schulmann et al., 1991; Dallmeyer et al., 1992; Misar and Urban, 1995; Büttner and Kruhl, 1997). Flysch deposition is interpreted to have resulted from rapid subsidence as a result of lithospheric loading by Moldanubian thrust sheets

[1] Inst. of Geology and Palaeontology, University, Hellbrunner Str. 34, A-5020 Salzburg, Austria. <franz.neubauer@sbg.ac.at>
[2] Dept. of Geology, University of Georgia, Athens/GA 30 602, USA.
[3] Inst. of Geology and Palaeontology, University, Heinrichstr. 26, A-8010 Graz, Austria.

0036-7699/03/0083/317

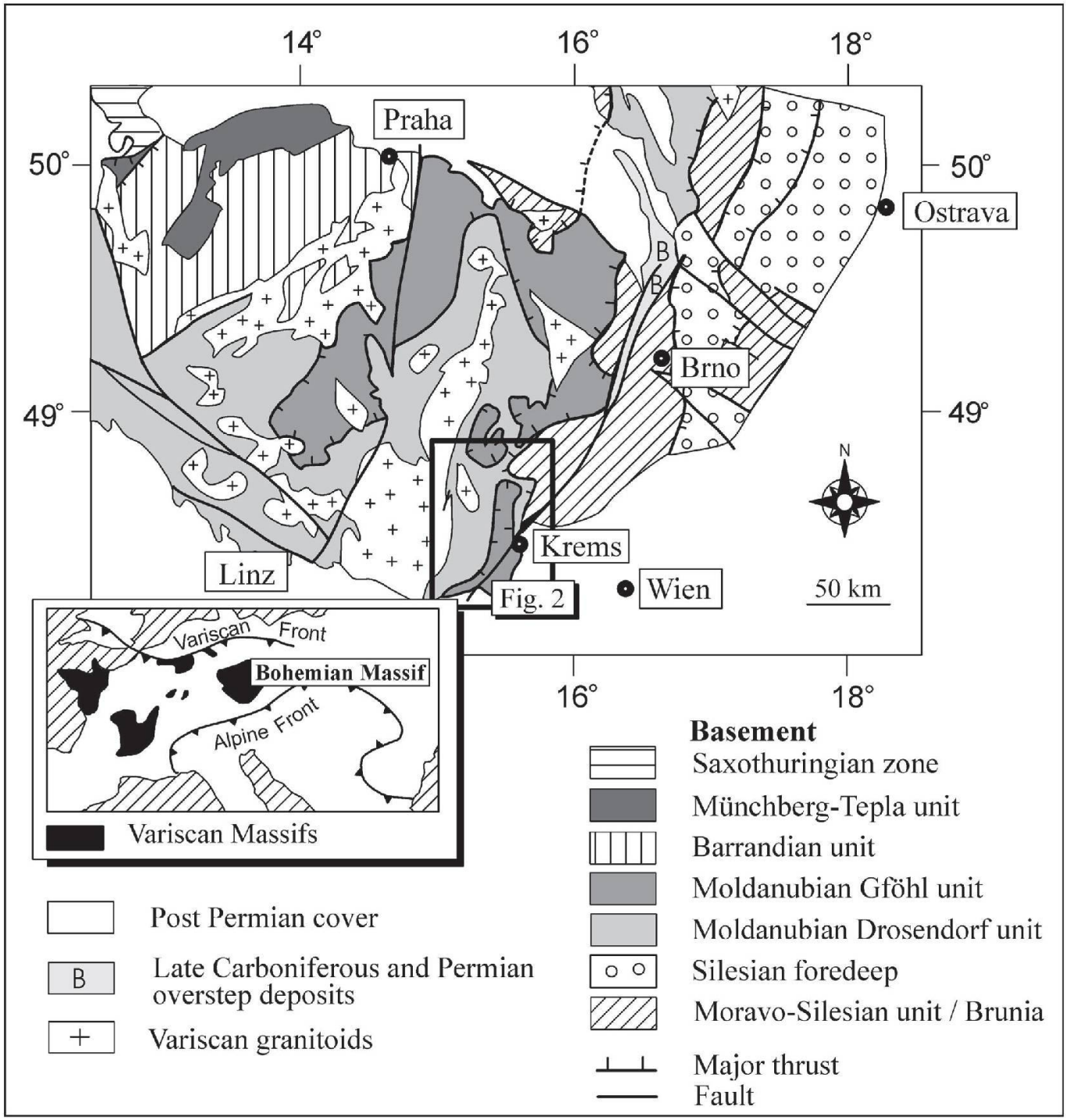

Fig. 1 Generalised geological map of the Bohemian Massif indicating the location of the present study area.

during the Early Carboniferous (e. g., Dallmeyer et al., 1992; Fritz and Neubauer, 1993). The Moldanubian nappe complex includes granulite-peridotite assemblages in the uppermost tectonic level and comprises several metamorphic sequences which were assembled prior to final emplacement of the entire nappe complex in the Early Carboniferous. Entrainment of asthenosphere-derived mantle rocks (garnet peridotites, pyroxenites) into subducted continental sequences (now granulites) is interpreted to have occurred during Early Carboniferous subduction (Becker, 1997; Brueckner, 1998). In the southeastern Bohemian Massif, the Moravo-Silesian and Moldanubian nappe complexes are penetratively foliated and metamorphosed. In the Moravo-Silesian unit, the metamorphic overprint increases southward (e.g., Höck, 1995) and westward towards the Moldanubian units. Peak conditions of metamorphism and subsequent cooling and deformation occurred during the Early Carboniferous (Matte et al., 1990; Dallmeyer et al., 1992; Vrána et al., 1995) in a dextral transpressive deformation regime (e.g., Schulmann et al., 1991; Fritz and Neubauer, 1993).

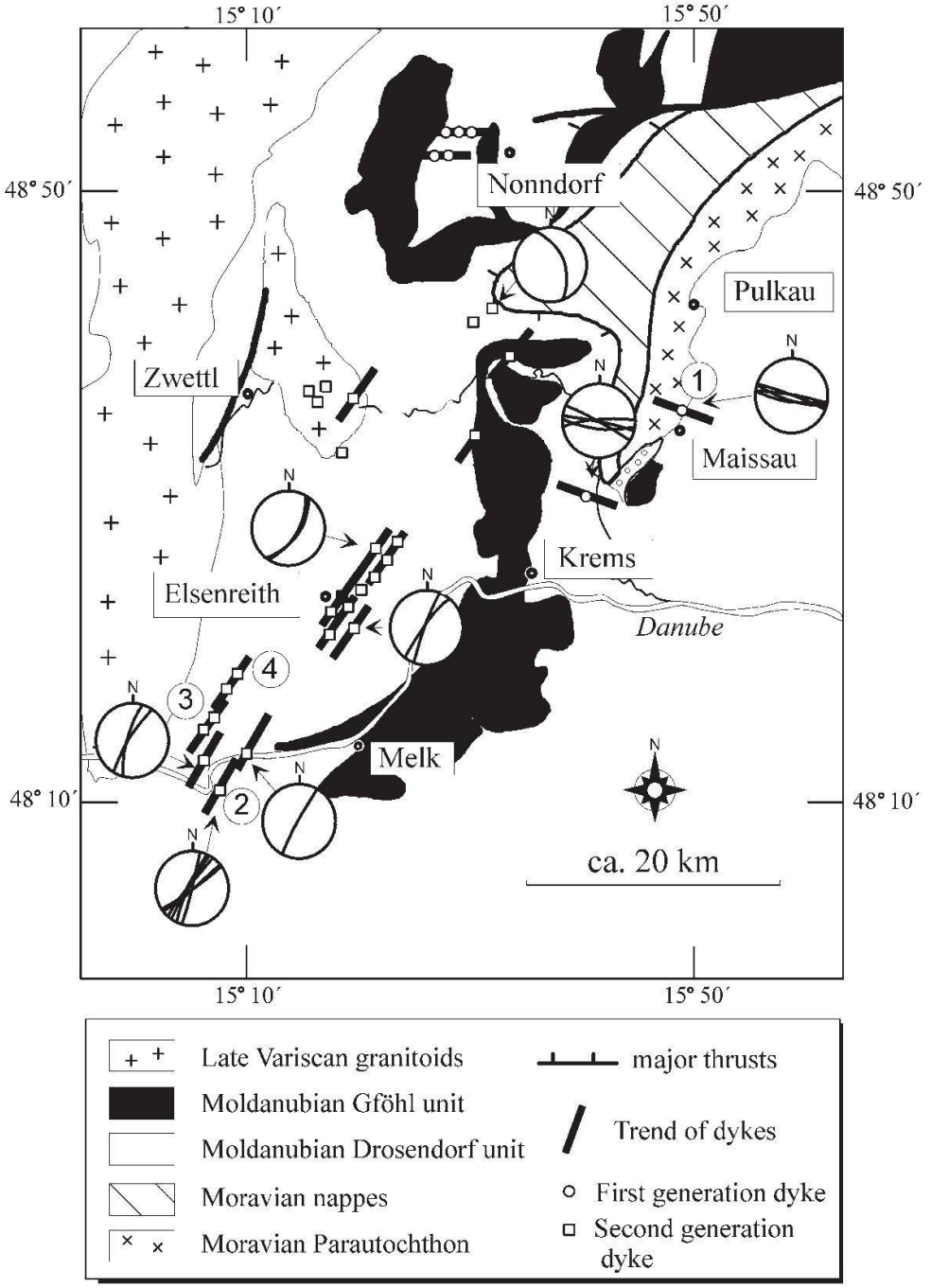

Fig. 2 Distribution of syn- and post-orogenic lamprophyric dykes in the southeastern Bohemian Massif. Open circles: foliated and metamorphic dykes (first lamprophyre generation); open squares: unfoliated and unmetamorphic dykes (second generation). Thick lines represent mapped dykes. Stereographic projections (lower hemisphere) represent great circles of measured dyke orientations. Numbers refer to locations sampled for $^{40}Ar/^{39}Ar$ dating.

Moldanubian units were uniformly metamorphosed during the Early Carboniferous, with P–T conditions of ca. 10–12 kbar and 750 °C following an earlier high pressure metamorphic stage (Vrána et al., 1995; Büttner and Kruhl, 1997, Cooke, 2000, and references listed therein). U–Pb zircon, monazite and Sm–Nd mineral data indicate that the peak of metamorphism occurred at ca. 350–335 Ma (Wendt et al., 1994; for full data compilation, see Fritz et al., 1996; Kröner et al., 2001). Becker (1997) reported Sm–Nd mineral ages ranging from ca. 352 ± 8 Ma to 329 ± 8 Ma from the uppermost Moldanubian nappes. Regional cooling through ca. 500 °C is recorded by $^{40}Ar/^{39}Ar$ amphibole ages of ca. 335 Ma, through 400–350 °C by muscovite ages of ca. 330 Ma, and through ca. 300 °C by 327–325 Ma biotite ages (Matte et al., 1985; Dallmeyer et al., 1992; Fritz et al., 1996). Post-metamorphic cooling was largely controlled by thrust loading of hot thrust sheets onto foreland successions (Dallmeyer et al., 1992; Fritz et al., 1996).

Emplacement of the composite South Bohemian batholith and the Rastenberg granodiorite

postdated penetrative internal Variscan deformation of the Moldanubian nappe complex and crosscut ductile thrust boundaries. U–Pb zircon and monazite crystallization ages of 328 ± 5 to 323 ± 4 Ma (Weinsberg Granite) and 328 ± 10 Ma (Rastenberg Granodiorite) suggest intrusion in the late Visean (Friedl, 1997; Gerdes, 2001; Finger et al., 1997 and references therein). Unfoliated and unmetamorphosed leucogranites yielded a Rb–Sr whole rock crystallization age of 332 ± 6 Ma (locality 2, Fig. 2; Frank et al., 1990). Leucogranitic dykes are cut by lamprophyres (Matura, 1984).

3. Distribution and field relationships of lamprophyre

The occurrences of lamprophyric dykes of the southeastern Bohemian Massif (Fig. 2) have been described by Neubauer and Fritz (1994). Two types of lamprophyre crosscut penetrative Variscan foliations in both Moldanubian and Moravo-Silesian units. The first type includes subvertical, variably metamorphosed and internally foliated dykes (locally described as Thuresit, Raabsit and Karlsteinit: e.g., Waldmann, 1951) which generally trend ESE. Metamorphic mineral assemblages (W of Nonndorf, Fig. 2) include chlorite, epidote and calcite oriented along a weakly developed foliation, and appear to have formed during a lower greenschist facies metamorphic overprint (ca. 350–400 °C). Unmetamorphosed, ESE-trending lamprophyres occur further east. The second type of dykes forms a set of NNE-trending nonfoliated and unmetamorphic lamprophyres; these have locally been described as kersantite, spessartite, minette, and/or gabbro (Köhler, 1928; Matura, 1984; Frasl et al., 1990; Richter et al., 1991; Büttner and Kruhl, 1997). The majority of nonfoliated lamprophyric dykes are distributed within a narrow NNE-trending zone that extends ca. 70 km from the Danube to Maissau (Fig. 2). The dykes generally range between 0.3 and 8 metres in thickness, but they locally exceed a width of 8 metres. Several centimetres wide clinopyroxene-rich zones along some dyke margins indicate some compositional zoning. No chilled margins or globules have been observed in either dyke generation.

4. Petrography

The nonfoliated dykes are variable in texture and mineralogical composition. Generally, most dykes are homogeneous with minor megacrysts of biotite, clinopyroxene, plagioclase and/or subordinate amphibole. Compositional zoning locally occurs within ca. 10 cm thick bands subparallel to dyke boundaries. Marginal portions are relatively enriched in clinopyroxene and sharply separated from biotite-rich central bands. The fine-grained groundmass contains all of the above minerals and includes opaque minerals, and, locally, subordinate secondary calcite, chlorite and serpentine (e. g., Richter et al., 1991). Bulk compositions range from kersantite to spessartite (Matura, 1984; Richter et al., 1991) using the nomenclature proposed by Streckeisen (1979). Systematic variation in mineralogical composition within lamprophyric dykes occurs between central and southern areas. Central portions of dykes include significant amounts of amphibole (spessartite), which is progressively replaced by biotite in southern areas (kersantite).

Monzogabbros have been locally found in association with lamprophyres. They mainly com-

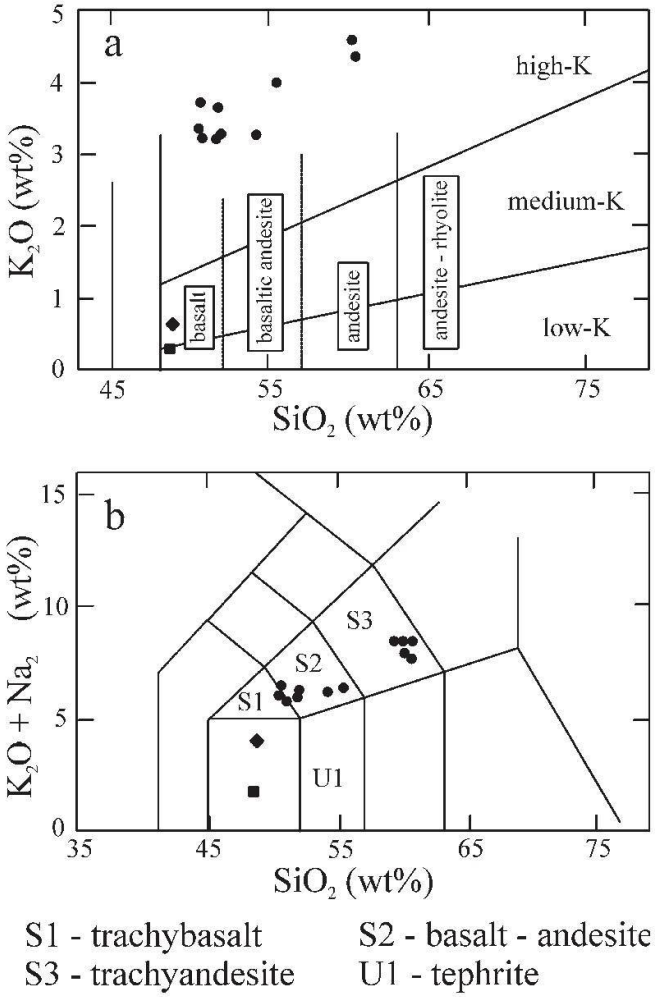

Fig. 3 Major element variations displaying series character (a) and rock classification (b) of dykes within the southeastern Bohemian Massif (according to systematics of LeMaitre, 1989). Open square: first generation dyke (only in b); filled circles: second generation lamprophyre; filled diamond: second generation monzogabbro.

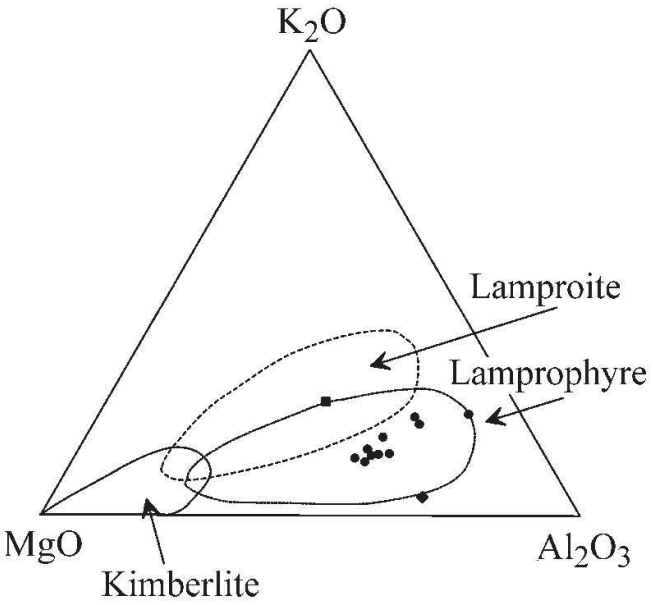

Fig. 4 Major element discrimination of ultrapotassic and potassic magmas (after Bergman, 1987). Data plotted as in Fig. 3.

prise millimetre-sized primary magmatic minerals including optically zoned and twinned plagioclase of intermediate composition, K-feldspar, biotite, olivine, orthopyroxene, clinopyroxene, skeletal opaque minerals and apatite. All mafic minerals have variably developed fine-grained reaction haloes. Olivine was mainly transformed to talc. Reaction haloes around pyroxene crystals include greenish amphibole. Brown magmatic biotite is often transformed into a fine-grained mixture of greenish biotite and opaque minerals.

Locally, decimetre thick lenses of trondhjemite and anorthosite occur within monzogabbro. Apart from a few grains of biotite and amphibole, these are composed of intermediate plagioclase, variable proportions of quartz, and accessory zircon.

5. Rock chemistry

A set of 17 samples was collected and chemically analysed after grinding in an agate mill and fusion of samples with $LiBO_2$ and HNO_3 dissolution. ICP-emission spectroscopy techniques were used for major and minor element, and Sc; ICP mass spectrometry was used for all other trace elements. Analyses were carried out at the Centre de Recherches Pétrographiques et de Géochimique à Vandoevre-lès-Nancy. Precision and accuracy were monitored using international rock standards.

One representative unmetamorphosed lamprophyre sample from the easternmost exposure of the first dyke generation, one monzogabbro and 15 lamprophyre samples from the second generation were analysed for major, minor and trace elements in order to evaluate the origin of parental magmas. Only unmetamorphosed and unaltered samples were selected. Results are listed in Table 1 and plotted in Figures 3–5.

Dykes from the second, NNE-trending generation display broad compositional variations reflected by positive covariation of silica vs. alkali contents (Fig. 3a, b). The high K_2O content (6.58 wt%) and high K_2O/Na_2O ratio (21.8) suggest that the first generation dyke sample is a tephrite of the ultrapotassic series (Bergman, 1987; Foley et al., 1987; Fig. 4). The generally high K contents

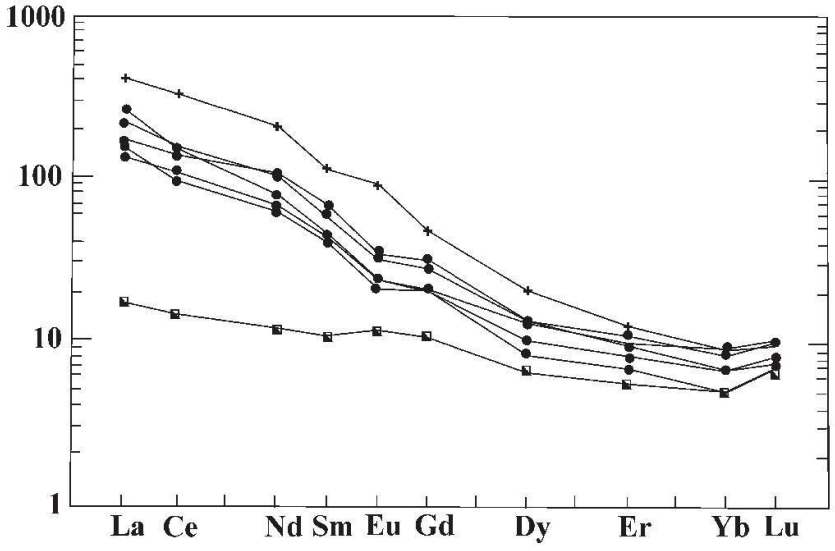

Fig. 5 REE patterns of generation 1 and 2 dykes. Normalisation values from Sun (1982). Legend: Cross: First generation sample (DA-AUST3D); circles: second generation mafic potassic and trachyandesitic dykes; half-filled quadrangle: monzogabbro from the second generation dykes.

Table 1 Chemical composition of lamprophyric dikes and related rocks in the southeastern Bohemian Massif. Sample DA-AUST-3D is a first generation dike, all others from the second generation. The samples of the second generation are ordered according to increasing Mg # number. Major and minor elements in weight percent, trace elements in ppm. LOI — loss of ignition.

Sample	DA-A-3D	JP9	JP7	JP11	JP8	JP16	JP28	JP20	JP1	JP4	JP19	JP5	JP3	JP17	JP14	JP13	JP2
SiO_2	45.31	60.17	60.75	60.75	59.45	48.71	48.50	51.95	60.45	54.20	51.84	50.52	50.65	55.42	51.67	50.96	60.20
TiO_2	2.33	0.93	0.91	0.91	0.93	1.58	0.80	1.06	0.63	0.93	1.16	1.01	1.02	0.96	1.11	1.11	0.64
Al_2O_3	10.88	16.73	16.73	16.71	16.70	15.38	18.78	15.05	14.71	14.48	14.03	14.91	14.91	13.61	14.13	13.61	14.58
FeO*	5.89	5.01	4.95	4.87	5.12	11.95	10.84	7.45	4.42	7.20	7.37	7.47	7.61	5.74	7.42	7.45	3.60
MnO	0.16	0.07	0.07	0.07	0.08	0.17	0.14	0.13	0.06	0.12	0.12	0.12	0.12	0.08	0.12	0.11	0.06
MgO	9.38	2.50	2.49	2.47	2.62	6.14	10.21	7.58	4.87	8.16	8.53	8.85	9.05	7.08	9.30	9.35	5.00
CaO	8.58	3.89	3.90	4.00	4.19	9.24	8.85	6.41	4.50	6.30	7.75	6.89	6.78	6.75	6.43	6.70	4.75
Na_2O	0.22	3.27	3.20	3.29	3.37	3.25	2.75	2.90	3.32	2.87	2.27	2.49	2.66	2.27	2.66	2.52	3.22
K_2O	6.58	5.09	5.04	5.05	5.00	0.65	0.27	3.25	4.37	3.27	3.65	3.37	3.72	4.00	3.22	3.22	4.58
P_2O_5	2.11	0.34	0.34	0.34	0.38	0.27	0.13	0.85	0.34	0.44	0.68	0.71	0.75	0.78	0.68	0.68	0.34
Total	91.44	98.00	98.38	98.46	97.84	97.34	98.27	96.63	97.67	97.97	97.40	96.34	97.27	96.69	96.74	95.71	96.97
LOI	7.09	0.99	0.61	0.54	0.55	1.08	0.32	2.42	1.11	1.07	1.68	1.92	1.26	1.48	2.09	2.84	0.89
Mg#	73.93	47.06	47.27	47.48	47.70	47.80	62.66	64.45	66.26	66.89	67.35	67.86	67.93	68.73	69.06	69.10	71.23
Cr	553	64	65	58	76	170	593	375	332	431	600	403	423	435	412	496	279
Ni	384	19	22	32	32	65	213	223	194	174	107	272	265	67	196	264	158
Co	40	73	69	36	57	55	72	43	95	49	43	55	58	34	40	47	60
Sc	22	14	14	13	13	26	20	23	13	20	26	23	23	25	21	21	14
V	148	58	57	58	71	238	160	149	101	131	146	157	161	157	132	125	96
Cu	49	13	14	15	25	77	54	30	80	27	94	56	57	29	27	23	4
Zn	100	72	66	68	75	100	88	87	60	91	72	93	77	60	76	88	64
K	–	42254	41839	41922	41507	5396	2241	26979	36277	27145	30300	27975	30881	33205	26730	26730	38020
Rb	288	209	211	199	217	19	10	142	143	140	173	149	169	184	139	124	122
Ba	7916	1381	1352	1323	1345	176	43	2614	2273	1667	1460	2116	2581	2439	2182	1673	2371
Sr	2458	480	481	478	483	360	204	963	1545	627	609	703	810	905	867	747	1649
Ga	19	18	18	30	25	31	8	5	15	17	15	43	34	11	15	14	28
Nb	33.0	4.0	4.0	4.0	4.0	4.0	4.0	4.0	4.0	4.0	4.0	9.0	8.0	4.0	4.0	4.0	4.0
Zr	893	350	347	348	338	104	44	280	231	223	235	264	258	288	230	230	238
Ti	–	5575	5455	5455	5575	9472	4796	6355	3777	5575	6954	6055	6115	5755	6654	6654	3837
Y	25	20	19	20	17	19	13	21	12	18	21	19	18	20	19	20	13
Th	–	27.00	32.00	29.00	38.00	26.00	4.00	42.00	46.00	27.00	46.00	66.00	61.00	45.00	48.00	47.00	48.00
La	136.29	44.23	44.06	–	–	–	5.64	–	84.74	50.63	55.27	–	–	–	–	70.50	–
Ce	283.60	93.16	94.98	–	–	–	12.67	–	131.40	81.16	118.90	–	–	–	–	132.90	–
Nd	130.74	40.72	42.65	–	–	–	7.47	–	50.18	39.16	67.41	–	–	–	–	65.21	–
Sn	22.48	9.04	8.79	–	–	–	2.22	–	9.08	8.24	13.91	–	–	–	–	12.17	–
Eu	6.98	1.82	1.85	–	–	–	0.90	–	1.81	1.63	2.71	–	–	–	–	5.51	–
Gd	13.23	6.03	5.92	–	–	–	2.98	–	5.70	5.68	8.58	–	–	–	–	7.79	–
Dy	9.05	4.62	4.44	–	–	–	2.26	–	2.9	3.5	4.7	–	–	–	–	4.67	–
Er	2.86	2.18	2.16	–	–	–	1.27	–	1.54	1.83	2.45	–	–	–	–	2.1	–
Yb	1.96	1.86	2.05	–	–	–	1.1	–	10.8	1.5	1.82	–	–	–	–	1.51	–
Lu	0.32	0.36	0.35	–	–	–	0.22	–	0.24	0.28	0.35	–	–	–	–	0.25	–

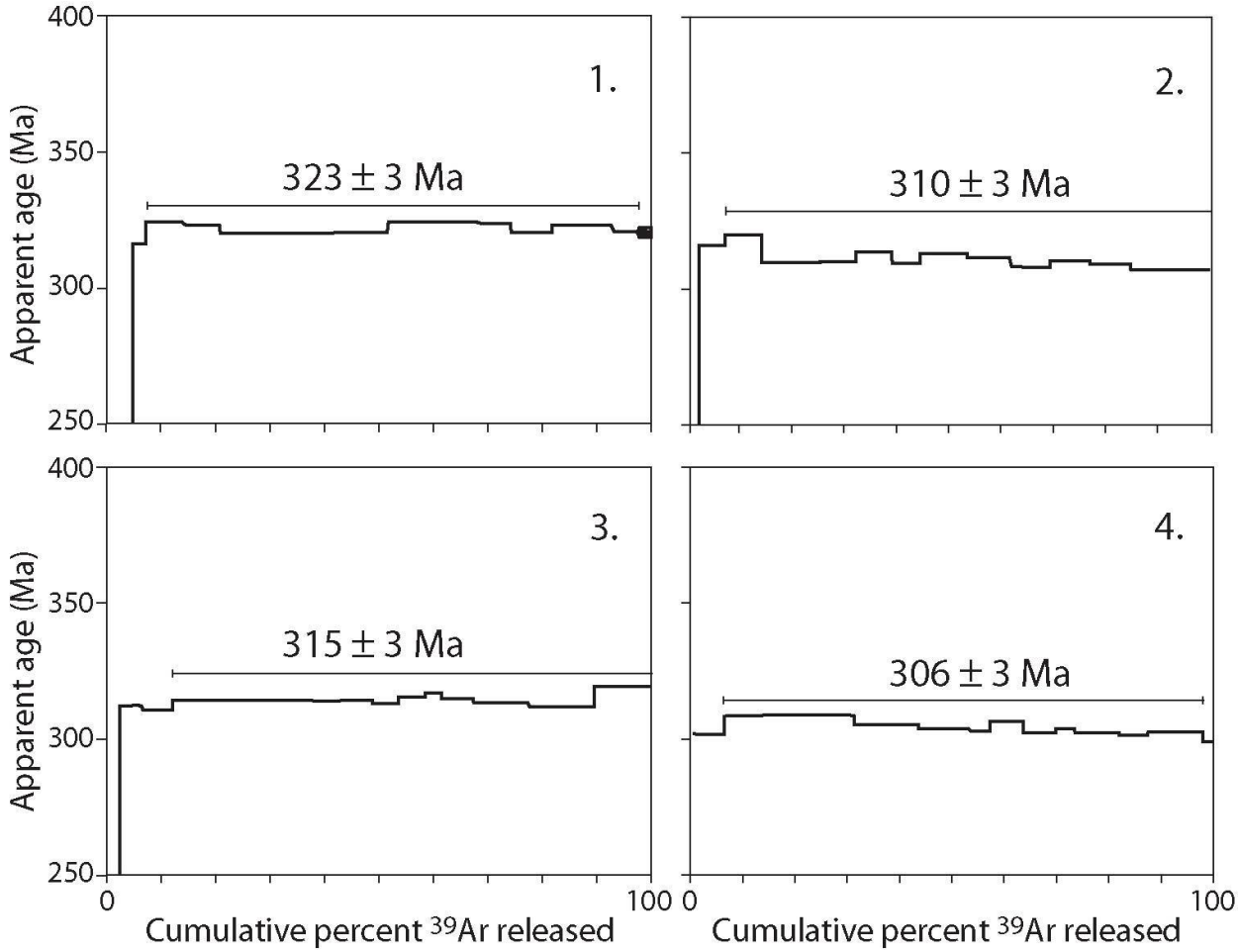

Fig. 6 $^{40}Ar/^{39}Ar$ release spectra of multi-grain biotite concentrates separated from samples of a first generation, SSE-trending dyke (sample 1) and second generation, NNE trending dykes (samples 2–4) of the southeastern Bohemian Massif. Experimental temperatures increase from left to right. Analytical uncertainties (two sigma, intralaboratory) are represented by vertical width of bars. Interlaboratory plateau ages are listed. For further explanation, see text.

of second generation dykes suggest a high-K (potassic) series (LeMaitre, 1989; Foley et al., 1987). Compositions range from trachybasalt, through basaltic trachyandesite to trachyandesite according to systematics proposed by LeMaitre (1989). Second generation dykes are enriched in Ba, Rb, Sr, Ni, Cr, P and light REEs, and depleted in Nb. Similarly, the monzogabbro sample is enriched in in Cr, Ni, P, T, and Zr. The degree of enrichment in light REEs of lamprophyres from the second generation is lower (as exemplified in REE patterns) within the first generation sample (Fig. 5). Interestingly, Nb is enriched in the first generation dyke, suggesting a significant difference in source origin between the two dyke generations. The La_N/Yb_N ratio is 46.5 within the first generation dyke sample, and between 31.2 and 15.9 (lamprophyres) and 3.59 (monzogabbro) within the second generation dykes. Eu anomalies are relatively weak and include small positive anomalies in first generation dyke and monzogabbro, and negative anomalies in second generation lamprophyres (Fig. 5). Sr isotopic characteristics ($^{86}Sr/^{87}Sr$ = 0.714) suggest that a major crustal component is included within mafic potassic and trachyandesitic magmas (Frank et al., 1990) of the second generation.

6. Argon dating

Mineral concentrates for $^{40}Ar/^{39}Ar$ analysis were wrapped in aluminium-foil packets, encapsulated in sealed quartz vials, and irradiated for 40 hours in the Central thimble position of the TRIGA Reactor at the U.S. Geological Survey, Denver. Variations in the flux of neutrons along the length of the irradiation assembly were monitored with several mineral standards, including MMhb-1 (Samson and Alexander, 1987). The samples were incrementally heated until fusion in a double-vacuum, resistance heated furnace. Temperature was monitored with a direct-contact thermocouple, controlled to ± 1 °C between increments, and isac-

Table 2 $^{40}Ar/^{39}Ar$ analytical data for incremental-heating experiments on biotite concentrates from post-Variscan lamprophyre dykes in the southeastern Bohemian Massif, Austria.

Release temperature (°C)	$(^{40}Ar/^{39}Ar)$ *	$(^{36}Ar/^{39}Ar)$ *	$(^{37}Ar/^{39}Ar)^C$	^{39}Ar % of total	% ^{40}Ar non-atmos.§	$^{36}Ar_{Ca}$ %	Apparent Age (Ma) ± Error **
Sample 1: J = 0.008933							
550	11.94	0.02665	0.372	0.71	34.25	0.38	64.7 ± 2.9
580	13.48	0.00888	0.754	3.68	80.93	2.31	167.7 ± 0.7
590	22.61	0.00375	0.094	2.73	95.11	0.68	316.8 ± 0.3
625	22.36	0.00066	0.009	6.57	99.11	0.36	325.7 ± 0.2
660	22.10	0.00017	0.008	6.81	99.75	1.31	324.2 ± 0.6
695	21.83	0.00017	0.005	8.34	99.74	0.85	320.6 ± 0.3
730	21.90	0.00041	0.009	11.92	99.43	0.59	320.5 ± 0.2
765	21.95	0.00045	0.025	10.34	99.37	1.52	321.1 ± 0.3
800	22.22	0.00033	0.026	5.75	99.54	2.13	325.1 ± 0.4
835	22.28	0.00060	0.011	11.20	99.18	0.49	324.8 ± 0.2
875	22.11	0.00028	0.008	6.13	99.61	0.76	323.9 ± 0.2
915	21.82	0.00024	0.010	7.18	99.65	1.12	320.1 ± 0.4
955	22.07	0.00045	0.009	11.35	99.37	0.57	322.7 ± 0.3
990	21.82	0.00012	0.025	4.90	99.82	5.72	320.6 ± 0.2
Fusion	21.83	0.00017	0.012	2.39	99.75	1.85	320.6 ± 1.8
Total	21.66	0.00097	0.045	100.00	98.21	1.21	314.8 ± 0.4
Total without 550–590 °C and fusion				90.49			322.5 ± 0.3
Sample 2: J = 0.008932							
490	12.84	0.01582	0.070	1.76	63.58	0.12	126.9 ± 0.8
540	22.09	0.00228	0.024	4.82	96.93	0.29	315.7 ± 0.5
580	22.10	0.00139	0.019	6.90	98.12	0.38	319.4 ± 0.6
625	21.06	0.00039	0.013	10.30	99.43	0.88	309.2 ± 0.4
660	21.11	0.00051	0.017	7.25	99.27	0.93	309.5 ± 0.1
695	21.54	0.00111	0.020	6.90	98.46	0.49	312.9 ± 0.4
730	21.22	0.00080	0.025	5.10	98.86	0.84	309.7 ± 0.8
770	21.64	0.00137	0.045	3.82	98.12	0.90	313.2 ± 0.2
840	21.50	0.00090	0.033	5.29	98.75	1.00	313.2 ± 0.2
955	21.30	0.00062	0.019	8.52	99.12	0.85	311.6 ± 0.2
895	21.13	0.00082	0.021	7.40	98.84	0.72	308.5 ± 0.6
935	21.06	0.00015	0.019	15.08	99.76	3.46	310.2 ± 0.4
Fusion	21.06	0.00060	0.041	16.41	99.14	1.84	308.5 ± 0.5
Total	21.18	0.00104	0.027	100.00	98.30	1.32	307.9 ± 0.4
Total without 550–590 °C and fusion				86.06			310.2 ± 0.4

curate to ± 5 °C. Measured isotopic ratios were corrected for total systems blanks and the effects of mass discrimination. Apparent $^{40}Ar/^{39}Ar$ ages were calculated from corrected isotopic ratios using decay constants and isotopic abundance ratios listed by Steiger and Jäger (1977).

A variety of uncertainties are associated with ages determined by incremental release, $^{40}Ar/^{39}Ar$ analyses. These include analytical uncertainties associated with the measurement of each isotopic ratio (inlet time extrapolation, mass discrimination correction, system blank, etc.) and overall uncertainties in age calculations (monitor age, atmospheric corrections, etc.). The latter are similar for each incremental age determination during analysis of one sample. Therefore, to evaluate potential differences in an incremental age analysis, only intralaboratory uncertainties should be considered. These have been calculated by rigorous statistical propagation of uncertainties associated with measurements of each isotopic ratio (at two standard deviations of the mean) through the age equation. Intralaboratory errors are listed in the data tables. Comparison of total-gas, plateau and/or isotope correlation ages between different samples and between different laboratories requires consideration of the total interlaboratory uncertainty. These are measured or calculated at ± 1.25–1.5% of the quoted age, and are given in the text. Total-gas ages were computed for each sample by appropriate weighting of the age and percent ^{39}Ar released within each temperature increment. A "plateau" is considered to be defined if the ages recorded by two or more contiguous gas fractions each representing >4 percent of the total ^{39}Ar evolved (and together constituting >50

Table 2 continued.

Release temperature (°C)	(^{40}Ar/^{39}Ar) *	(^{36}Ar/^{39}Ar) *	(^{37}Ar/^{39}Ar)^{C}	^{39}Ar % of total	% ^{40}Ar non-atmos.§	$^{36}Ar_{Ca}$ %	Apparent Age (Ma) ± Error **
Sample 3: J = 0.009392							
450	30.88	0.07218	0.216	0.25	30.96	0.08	155.1 ± 2.8
500	17.41	0.00555	0.076	1.76	90.58	0.37	249.2 ± 0.8
535	21.02	0.00271	0.016	4.16	96.17	0.16	313.6 ± 0.6
575	20.98	0.00284	0.019	5.40	95.98	0.18	312.4 ± 0.4
640	20.42	0.00027	0.021	11.25	99.59	2.12	315.3 ± 0.2
645	20.35	0.00011	0.013	10.27	99.81	3.03	314.9 ± 0.2
680	50.41	0.00030	0.021	6.83	99.54	1.85	315.0 ± 0.3
715	20.41	0.00030	0.021	8.24	99.55	1.89	315.0 ± 0.4
755	20.65	0.00124	0.030	4.79	98.21	0.65	314.4 ± 0.7
795	20.79	0.00127	0.057	5.31	98.19	1.23	316.3 ± 0.2
835	20.94	0.00155	0.037	2.99	97.80	0.64	317.2 ± 0.4
880	20.61	0.00076	0.037	5.66	98.89	1.32	315.9 ± 0.7
925	20.38	0.00023	0.036	10.28	99.65	4.27	314.9 ± 0.4
965	20.32	0.00045	0.038	12.27	99.34	2.31	313.1 ± 0.5
Fusion	20.72	0.00045	0.042	10.52	99.34	2.50	318.8 ± 0.6
Total	20.51	0.00097	0.031	100.00	98.65	2.03	313.6 ± 0.4
Total without 550–590°C and fusion				88.42			315.4 ± 0.4
SampIe 4: J = 0.008565							
500	27.65	0.02800	0.645	0.18	70.23	0.63	277.6 ± 2.0
550	23.69	0.00781	0.061	6.42	90.25	0.2	303.4 ± 0.6
590	22.14	0.00095	0.037	11.18	98.72	1.06	309.5 ± 0.3
625	21.97	0.00038	0.034	13.10	99.47	2.40	309.6 ± 0.2
650	21.84	0.00052	0.031	12.39	99.28	1.64	307.3 ± 0.3
695	21.73	0.00071	0.040	10.15	99.02	1.53	305.2 ± 0.6
735	21.84	0.00132	0.057	4.35	98.21	1.17	304.2 ± 0.6
780	21.82	0.00035	0.046	5.65	99.51	3.55	307.7 ± 0.3
825	21.48	0.00031	0.059	5.86	99.57	5.13	303.5 ± 0.5
870	21.48	0.00025	0.074	12.62	99.66	8.11	303.7 ± 0.7
910	21.57	0.00064	0.104	4.87	99.14	4.46	303.4 ± 0.3
930	21.51	0.00013	0.128	10.98	99.84	26.37	304.6 ± 0.2
Fusion	21.24	0.00020	0.325	2.26	99.81	43.72	301.1 ± 0.2
Total	21.28	0.00102	0.066	100.00	98.68	6.48	305.9 ± 0.4
Total without 550–590°C and fusion				91.14			306.3 ± 0.4

* measured.
c corrected for post-irradiation decay of ^{37}Ar (35.1 day half-life).
§ $[^{40}Ar_{tot} - (^{36}Ar_{atmos})\ (295.5)] / {}^{40}Ar_{tot}$.
** calculated using correction factors of Dalrymple et al. (1981); two sigma, intralaboratory errors.

percent of the total quantity of ^{39}Ar evolved) are mutually similar to within a ±1% intralaboratory uncertainty. Analysis of the MMhb-1 amphibole monitor indicates that apparent K/Ca ratios may be calculated through the relationship 0.518 (± 0.005) x $(^{39}Ar/^{37}Ar)_{corrected}$.

Plateau portions of the analyses were plotted on ^{36}Ar/^{40}Ar vs. ^{39}Ar/^{40}Ar isotope correlation diagrams (Roddick et al., 1980). Regression techniques followed the methods of York (1969). A mean square of the weighted deviates (MSWD) is the statistical parameter which has been used to evaluate isotopic correlations. Roddick (1978) suggested that a MSWD > ca. 2.5 indicates scatter about a correlation line greater than can be explained by experimental errors alone. Time-scale calibration follows the recent compilation of Remane (2000).

One biotite concentrate was prepared from a representative sample collected within a first generation ESE-trending dyke (tephrite). Three biotite concentrates were separated from three NNE-trending dykes. Sample locations are shown on Fig. 2. Analytical results are presented in Table 2 and are displayed as age spectra in Fig. 6.

The four biotite concentrates are characterised by plateau ages which include between ca. 90 to 85 percent of the experimentally evolved ^{39}Ar. No extraneous argon component was detected in the ^{36}Ar/^{40}Ar–^{39}Ar/^{40}Ar isotope correlation. Bi-

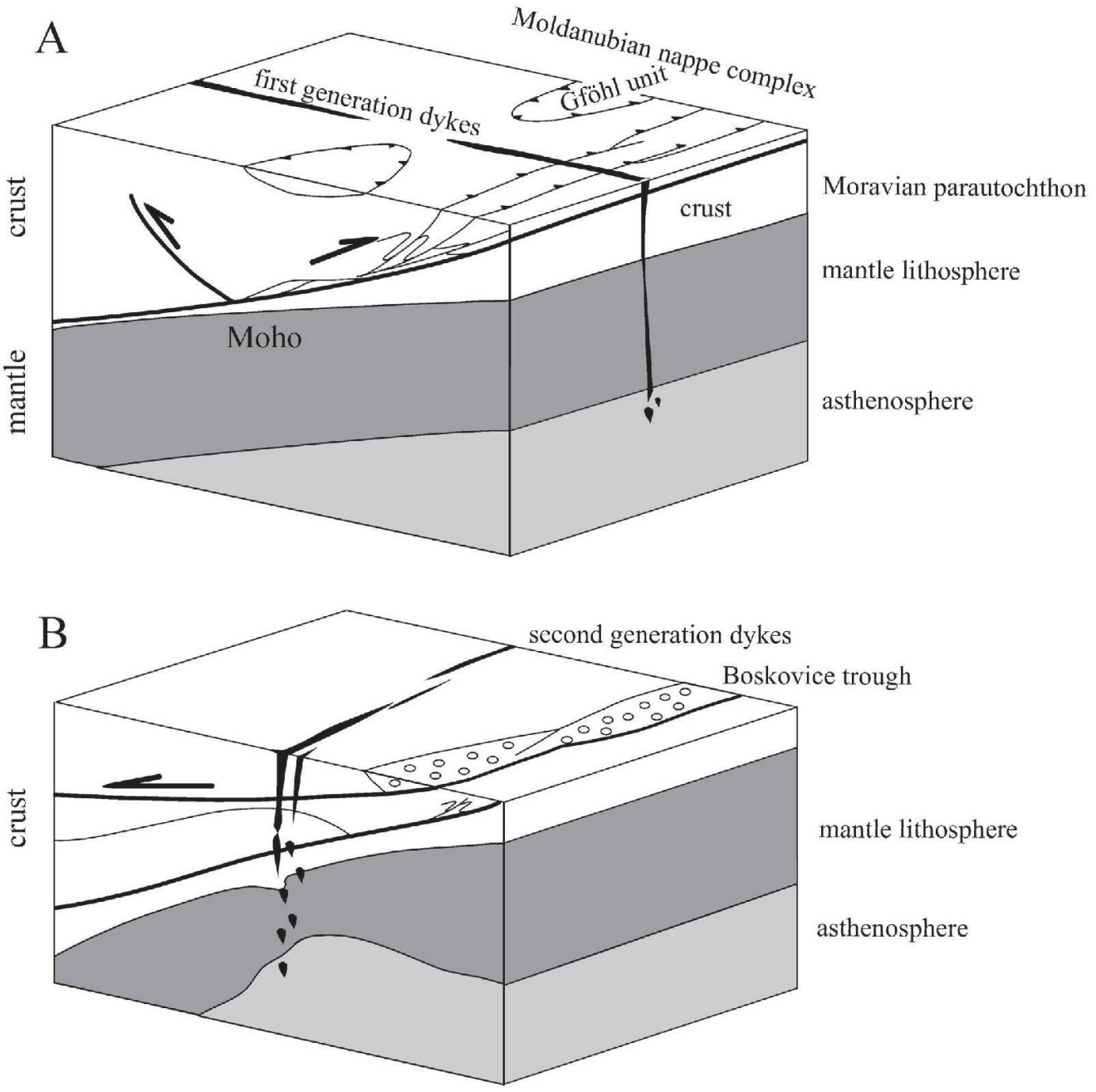

Fig. 7 Possible relationships between origin of potassic magmas in the Bohemian Massif and extension within the Alpine realm: A—Intrusion of first generation lamprophyric dykes in a contractional regional setting. B—Intrusion of second generation lamprophyric dykes into an extensional regional setting associated with slab roll-back and subsequent slab break-off, and thermal relaxation of subducted lithosphere within an overall continental collisional setting.

otite from sample 1 (first generation dyke) records a $^{40}Ar/^{39}Ar$ plateau age of 323 ± 3 Ma. The three biotite concentrates from the second generation dykes record plateau ages of 316 ± 3 Ma, 310 ± 3 Ma, and 306 ± 3 Ma.

7. Discussion

Field relationships indicate that the lamprophyric dykes intruded into a previously assembled Variscan nappe succession. Detailed structural work indicates that thrusting occurred concomitant with peak temperature conditions (e. g., Fritz et al., 1996). Local retrogression occurred at upper amphibolite facies and greenschist facies conditions along detachment faults only, related to the exhumation of the Moldanubian nappe assembly (Neubauer, 1990; Stipska and Schulmann, 1995; Fritz et al., 1996; Büttner and Kruhl, 1997). Peak metamorphic conditions within the granulite nappes are estimated to have been attained at ca. 345–335 Ma (Wendt et al., 1994; Becker, 1997). Deformation appears to have been associated

with upthrusting of hot granulite nappes and emplacement onto cool rocks of the lower continental structural sequence. This resulted in an inversion of the metamorphic gradient (Stipska and Schulmann, 1995; Fritz et al., 1996). Dykes appear to have been emplaced into a still warm crust, as indicated by partial greenschist metamorphic overprint on western first generation dykes, and the absence of globules (ocelli) and chilled margins in the second generation of dykes.

Petrographic and geochemical characteristics of the lamprophyric dykes indicate that they belong, respectively, to an ultrapotassic suite (first generation), and a potassic series (second generation). Such rocks form within various tectonic settings, but they are especially common in continental crust when parental magmas were derived from deep-seated, lithospheric or asthenospheric sources, where garnet residues play a major role (Bergman, 1987; Foley et al., 1987; Wilson, 1991; Shand et al., 1994; Mitchell, 1994; Turner et al., 1996). Strong enrichment of incompatible elements, together with elevated concentrations of elements (e.g., Mg, Cr, Ni) derived from mantle rocks, suggests that a very low-melt percentage was derived from the asthenosphere. The compositions of second generation dykes argue for an origin from a similarly enriched mantle, however with a major but variable lithospheric influence from a subduction-related environment. The monzogabbro may be explained by strong fractionation from parental magmas of the second generation parental magma.

The orientation of the dykes, together with their state of deformation and metamorphism, indicates emplacement of two generations of lamprophyric dykes in response to a change in the external stress field. The first dyke generation trends ESE, the second NNE. The only exceptions are dykes from the Maissau quarry (Fig. 2), where ESE-trending and unmetamorphic dykes are exposed at the margin to the Variscan metamorphic area of the southeastern Bohemian Massif, in which the metamorphic overprint generally increases westwards (Höck et al., 1990; Höck, 1995; Vrána et al., 1995). $^{40}Ar/^{39}Ar$ muscovite ages from granitic rocks of the Pulkau area (Fig. 2) record only partial Variscan rejuvenation of Cadomian mineral ages (Fritz et al., 1996). Therefore, the Maissau dyke is interpreted to be part of the first generation, ESE-trending dykes which were emplaced at the periphery of a Variscan metamorphic dome located to the west.

$^{40}Ar/^{39}Ar$ ages recorded by muscovite and hornblende (Dallmeyer et al., 1992; Fritz et al., 1996), combined with Rb–Sr muscovite and biotite dates (Matte et al., 1985; Morauf and Jäger, 1982), and $^{40}Ar/^{39}Ar$ biotite data (Matte et al., 1985) indicate rapid cooling of the assembled Moldanubian/Moravian nappe complexes (from >500 °C to ca. 300 °C between ca. 335 and 320 Ma). Cooling was locally accompanied by ductile deformation within a dextral transpressive zone (e. g., Dallmeyer et al., 1992; Fritz and Neubauer, 1993). Therefore, dyke emplacement must have occurred between ca. 335–320 Ma, following penetrative Variscan deformation of country rocks which were only locally affected by subsequent deformation within discrete ductile shear zones. Emplacement of the first generation lamprophyric dykes may have been synchronous with the crustal shortening expressed by open, ESE-vergent folds (Fuchs and Matura, 1976; Tollmann, 1982; Weber and Duyster, 1990; Neubauer and Fritz, 1994). Internal deformation could have resulted from subhorizontal coaxial shortening which also led to development of folds in some areas (Fig. 7A). The $^{40}Ar/^{39}Ar$ biotite plateau recorded by the first generation dyke age suggests that initial dyke intrusion was associated with final shortening, exhumation and cooling through ca. 300 °C prior to ca. 322 Ma. This age for final shortening is also constrained by deformation within the Silesian peripheral foreland basin where final shortening occurred at the Viséan-Namurian boundary (ca. 320 Ma, using calibrations of Gradstein and Ogg, 1996, Remane, 2000; Dvorák, 1995; Cizek and Tomek, 1991; Fig. 7A).

The timing and tectonic significance of nonfoliated, second generation dykes are more difficult to assess. Emplacement of the "Waldviertel dyke swarm" postdated regional metamorphism and deformation, indicating a maximum emplacement age of ca. 325–320 Ma. Their emplacement predates the leucogranite dykes which are crosscut by unfoliated lamprophyric dykes (Matura, 1984). Leucogranite dykes record Rb–Sr whole-rock crystallisation ages of 332 ± 6 Ma (Frank et al., 1990). Emplacement of non-foliated dykes was apparently unrelated to trends of structures within the Variscan nappe, although they trend subparallel to nappe units within the southeastern Bohemian Massif. Variations in biotite ages from one cogenetic dyke swarm argue that the dykes intruded into a crust that was still warm, and that the ages date variable regional cooling to below ca. 300 °C. We therefore infer a close relationship between extension at upper lithospheric levels (expressed by the formation of the NNE-trending Boscovice trough which is filled with Westfalian to Early Permian clastic sediments; Fig. 1), and ESE-displacing, greenschist facies low angle normal faults observed in the study area (Neubauer, 1990). Together, these structures constrain ESE-

WNW stretching of crust during late stages of the orogenic evolution (Fig. 7B).

8. Regional tectonic significance

Simple shear models developed for the evolution of rifts have been used to explain volcanism and emplacement of subvertical, mafic to intermediate dykes in upper plate positions and subparallel to rift margins (e.g., Wernicke, 1985; Voggenreiter et al., 1988). Applying these concepts to the southeastern Bohemian Massif, the lamprophyric dykes could trace extension within an upper plate situated above a major detachment fault. On the other hand, post-orogenic lamprophyres occur in many orogens, especially in the entire European Variscan belt (Bergman et al., 1987; Foley et al., 1987; Turpin et al., 1988; Turner et al., 1996; Hegner et al., 1998; Bea et al., 1999; Propach, 2002) although anorogenic plume-lithosphere interaction is also suggested as an origin of some lamprophyres (e.g., Le Roex and Lanyon, 1998). In orogens, lamprophyres have been explained as deriving from the asthenosphere where magma uprises after convective removal of subducted lithosphere (e. g., Turner et al., 1996) or by delamination after slab break-off of the subducted lithosphere within collisional tectonic settings (e. g., Royden, 1993; von Blanckenburg and Davies, 1995; Davies and von Blanckenburg, 1995). Such a scenario may be appropriate for the evolution of the southeastern Bohemian Massif because chemical characteristics of the dykes indicate mixed asthenospheric or more lithospheric mantle sources for lamprophyric melts (Fig. 7B). The timing of Variscan continental collision is constrained by: (1) the onset of subsidence within the Silesian foreland basin at the base of the Lower Visean (ca. 350 Ma using the time-scale of Gradstein and Ogg, 1996); and (2) peak conditions within upper plate granulites (ca. 345–340 Ma: e.g., Wendt et al., 1994; Becker, 1997). This suggests that ca. 20–10 Ma elapsed between continental collision and subsequent intra-orogenic extension associated with convective removal of the subducted lithosphere or slab break-off. Similar time intervals have been deduced from other orogens, such as the Himalayan-Tibetan system (Turner et al., 1996) or the Cenozoic Alpine collisional belt, where the time interval between continental collision and slab break-off is estimated at ca. 20 Ma (e.g., von Blanckenburg and Davies, 1995).

Intrusion of asthenospheric dykes requires a mechanically stiff, brittle lithosphere with a deep-seated effective elastic thickness of the lithosphere (Cloetingh and Burov, 1996). Such rheological behaviour is expected only in external portions of orogens where the lower lithosphere has not been thoroughly thermally rejuvenated during contraction. This appears to have been the case within the southeastern Bohemian Massif where the Variscan granulite nappe structurally overrode the lower grade Moldanubian nappe sequence and represented an important heat source for regional metamorphism during continental collision. The thermal input is interpreted to have been dissipated through heating of the underlying, relatively cooler units, and suggested lithospheric rollback effects after slab-break-off according to models proposed by Royden (1993).

Mafic to intermediate magmas of high density only ascend to high crustal levels when magma uprise is driven by high lithostatic pressure exerted on a deep-seated magma chamber and when the uprising magma is in connection with the magma chamber (Suppe, 1985). The density of investigated lamprophyres is between 2.75 and 2.8 kg/m^3, significantly higher than 2.65–2.70 kg/m^3 of all other, acidic lithologies of the Bohemian Massif (Lenz et al., 1996). Assuming a low internal fluid pressure (or fluid pressure in equilibrium with lithospheric hosts rocks) and open connections between primary magma chambers and magma during dyke emplacement, the high density contrast between intermediate to mafic dykes and acidic crustal host rocks also argues for a relatively deep origin for parental magmas within the lithospheric mantle or at its base.

Acknowledgements

The paper benefited from discussions with Thomas Menzel and from remarks to an earlier version of the manuscript by Simon Kelley, and formal reviews and remarks by Paddy O'Brien, an anonymous reviewer, Urs Schaltegger and Martin Engi. We acknowledge financial support by a grant of the Austrian Research Foundation (P4713-GEO) to FN and HF, and by the Tectonics Program (EARTH 9316042) of the US National Science Foundation to RDD.

References

Bea, F., Monetro, P. and Molina, J.F. (1999): Mafic precursors, peraluminous granitoids, and late lamprophyres in the Avila batholith: a model for the generation of Variscan batholiths in Iberia. *J. Geol.* **107**, 399–419.

Becker, H. (1997): Sm–Nd garnet ages and cooling history of high-temperature garnet peridotite massifs and high-pressure granulites from lower Austria. *Contrib. Mineral. Petrol.* **127**, 224–236.

Bergman, S.C. (1987): Lamproites and other potassium-rich igneous rocks: a review of their occurrence, mineralogy and geochemistry. In: Fitton, J.G. and Upton,

B.G.J. (eds.): Alkaline igneous rocks. *Geol. Soc. London Spec. Publ.* **30**, 103–189.

Blanckenburg, F. von and Davies, J.H. (1995): Slab break-off: A model for syncollisional magmatism and tectonics in the Alps. *Tectonics* **14**, 120–131.

Brueckner, H.K. (1998): Sinking intrusion model for the emplacement of garnet-bearing peridotites into continental collision orogens. *Geology* **26**, 631–634.

Büttner, S. and Kruhl, J.H. (1997): The evolution of a late-Variscan high-T/low-P region: the southeastern margin of the Bohemian massif. *Geol. Rundsch.* **86**, 21–38.

Cizek, P. and Tomek, C. (1991): Large-scale thin-skinned tectonics in the eastern boundary of the Bohemian Massif. *Tectonics* **10**, 273–286.

Clemens, J.D. and Mawer, C.W. (1992): Granitic magma transport by fracture propagation. *Tectonophysics* **204**, 339–360.

Cloetingh, S. and Burov, E.B. (1996): Thermomechanical structure of European continental lithosphere: constraints from rheological profiles and EET estimates. *Geophys. J. Internat.* **124**, 695–723.

Cooke, R.A. (2000): High-pressure/temperature metamorphism in the St. Leonhard Granulite Massif, Austria: evidence from intermediate pyroxene-bearing granulites. *Int. J. Earth Sci.* **89**, 631–651.

Dallmeyer, R.D., Neubauer, F. and Hoeck, V. (1992): Chronology of late Paleozoic tectonothermal activity in the southeastern Bohemian Massif, Austria (Moldanubian and Moravo-Silesian zones): $^{40}Ar/^{39}Ar$ age controls. *Tectonophysics* **210**, 135–153.

Davies, J.H. and Blanckenburg, F. von (1995): Slab break-off: A model of lithosphere detachment and its test in the magmatism and deformation of collisional orogens. *Earth Planet. Sci. Lett.* **129**, 85–102.

Dvorák, J. (1995): Moravo-Silesian Zone – Autochthon – Stratigraphy. In: Dallmeyer, R.D., Franke, W. and Weber, K. (eds.): Pre-Permian Geology of Central and Eastern Europe. Springer-Verlag, Berlin, pp. 577–489.

Emerman, S.H. and Marrett, R. (1990): Why dikes? *Geology* **18**, 231–233.

Finger, F., Roberts, M.P., Haunschmid, B., Schermaier, A. and Steyrer, H.P. (1997): Variscan granitoids of central Europe: their typology, potential sources and tectonothermal relations. *Mineral. Petrol.* **61**, 67–96.

Foley, S.F., Venturelli, G., Green, D.H. and Toscani, L. (1987): The ultrapotassic rocks: characteristics, classification and constraints for petrogenetic models. *Earth Sci. Rev.* **24**, 81–134.

Frank, W., Hammer, S., Popp, F., Scharbert, S. and Thöni, M. (1990): Isotopengeologische Neuergebnisse zur Entwicklungsgeschichte der Böhmischen Masse: Proterozoische Gesteinsserien und variszische Metamorphose. *Österr. Beitr. Meteorolog. Geophysik* **3**, 185–228.

Franke, W. (1989): Tectonostratigraphic units in the Variscan belt of central Europe. *Geol. Soc. Am. Spec. Pap.* **230**, 67–90.

Frasl, G., Höck, V. and Finger, F. (1990): The Moravian zone in Austria. In: Franke, W. (ed.): Bohemian Massif. IGCP no. 233, Terranes in the circum-Atlantic Paleozoic Orogens. Field Guide Bohemian Massif, 127–142, Göttingen-Giessen.

Friedl, G. (1997): U/Pb-Datierungen an Zirkonen und Monaziten aus Gesteinen vom österreichischen Anteil der Böhmischen Masse. PhD thesis University of Salzburg, 242 pp.

Fritz, H. and Neubauer, F. (1993): Kinematics of crustal stacking and dispersion in the south-eastern Bohemian Massif. *Geol. Rundsch.* **82**, 556–565.

Fritz, H., Dallmeyer, R.D. and Neubauer, F. (1996): Thick-skinned versus thin-skinned thrusting: rheology-controlled thrust propagation in oblique collisional belts: the Southeastern Bohemian Massif (Czech Republic–Austria). *Tectonics* **15**, 1389–1413.

Fuchs, G. and Matura, A. (1976): Die Geologie des Kristallins der südlichen Böhmischen Masse. *Jahrb. Geol. Bundesanst. Wien* **119**, 1–43.

Gerdes, A. (2001): Magma homogenisation during anatexis, ascent and/or emplacement? Constraints from the Variscan Weinsberg Granites. *Terra Nova* **13**, 305–312.

Gerdes, A., Wörner, G. and Henk, A. (2000): Post-collisional granite generation and HT-LP metamorphism by radiogenic heating: the Variscan South Bohemian Batholith. *J. Geol. Soc. London* **157**, 577–587.

Gradstein, F.M. and Ogg, J. (1996): A Phanerozoic time scale. *Episodes* **19**, 3–4.

Hegner, E., Kölbl-Ebert, M. and Loeschke, J. (1998): Post-collisional Variscan lamprophyres (Black Forest, Germany): $^{40}Ar/^{39}Ar$ phlogopite dating, Nd, Pb, Sr isotope, and trace element characteristics. *Lithos* **45**, 395–411.

Höck, V. (1995): Moravo-Silesian Zone – Metamorphic evolution. In: Dallmeyer, R.D., Franke, W. and Weber, K. (eds.): Pre-Permian Geology of Central and Eastern Europe. Springer-Verlag, Berlin, pp. 541–553.

Höck, V., Marschallinger, R. and Topa, D. (1990): Granat-Biotit-Geothermometrie in Metapeliten der Moravischen Zone in Österreich. *Österr. Beitr. Meteorol. Geophysik* **3**, 149–167.

Köhler, A. (1928): Zur Kenntnis der Ganggesteine im niederösterreichischen Waldviertel. *Tschermaks Mineral. Petrograph. Mitt.* **39**, 125–213.

Kröner, A., O'Brien, P.J., Nemchin, A.A. and Pidgeon, R.T. (2001): Zircon ages for high pressure granulites from South Bohemia, Czech Republic, and their connection to Carboniferous high temperature processes. *Contrib. Mineral. Petrol.* **138**, 127–142.

Lenz, B., Mauritsch, H.J. and Reisinger, J.R. (1996): Petrophysical investigations in the Southern Bohemian Massif (Austria): data-aquisition, -organisation and -interpretation. *Mineral. Petrol.* **58**, 279–300.

LeMaitre, R.W. (ed.) (1989): A classification of igneous rocks and glossary of terms. Blackwell, Oxford, 193 pp.

Le Roex, A.P. and Lanyon, R. (1998): Isotope and Trace Element Geochemistry of Cretaceous Damaraland lamprophyres and carbonatites, Northwestern Namibia: Evidence for Plume-Lithosphere Interactions. *J. Petrol.* **39**, 1117–1146.

Matte, Ph., Maluski, H. and Echtler, H. (1985): Cisaillements ductile vers l'Est–Sud Est dans les nappes du Waldviertel (Sud-Est du Massif de Boheme, Autriche). Données microtectoniques et radiometriques $^{39}Ar/^{40}Ar$. *C. Rend. Acad. Sci. Paris* **301** (2/10), 721–726.

Matte, Ph., Maluski, H., Rajlich, P. and Franke, W. (1990): Terrane boundaries in the Bohemian Massif: Result of large-scale Variscan shearing. *Tectonophysics* **177**, 151–170.

Matura, A. (1984): Das Kristallin am Südrand der Böhmischen Masse zwischen Ybbs/Donau und St. Pölten. *Jahrb. Geol. Bundesanst. Wien* **127**, 13–27.

Misar, Z. and Urban, M. (1995): Moravo-Silesian Zone – Introduction. In: Dallmeyer, R.D., Franke, W. and Weber, K. (eds.): Pre-Permian Geology of Central and Eastern Europe. Springer-Verlag, Berlin, pp. 469–473.

Mitchell, R.H. (1994): The lamprophyre facies. *Mineral. Petrol.* **51**, 137–146.

Morauf, W. and Jäger, E. (1982): Rb–Sr whole rock ages for the Bites Gneiss, Moravicum, Austria. *Schweiz. Mineral. Petrograph. Mitt.* **62**, 327–334.

Neubauer, F. (1990): Kinematics of Variscan deformation in the Moldanubian zone, southern Bohemian Massif: Preliminary results from the Danube section. *Österr. Beitr. Meteorol. Geophysik* **3**, 57–76.

Neubauer, F. and Fritz, H. (1994): Syn- and post-orogenic lamprophyric dyke systems in the southeastern Bohemian Massif. *N. Jahrb. Geol. Paläont. Monatshefte* 1994, 476–486.

Price, N.J. and Cosgrove, J.W. (1990): Analysis of geological structures. Cambridge University Press, Cambridge, 502 pp.

Propach, G. (2002): Postmagmatic mineral parageneses of dikes may be used to estimate the PT data of their country rocks – An example from the Bayrischer Wald, Germany. *N. Jahrb. Mineral. Monatshefte* 2002/9, 424–432.

Remane, J., ed. (2000): Explanatory note to the international stratigraphic chart. UNESCO, Division of Earth Sciences, Paris, pp. 1–16.

Richter, W., Koller, F. and Beran, A. (1991): Exkursion in die metamorphen Serien und magmatischen Gesteinskomplexe des Waldviertels, Moldanubikum, Österreich. *Beihefte Europ. J. Mineral.* **1991**/2, 131–159.

Roddick, J.C. (1978): The application of isochron diagrams in $^{40}Ar/^{39}Ar$ dating: a discussion. *Earth Planet. Sci. Lett.* **41**, 233–244.

Roddick, J.C., Cliff, R.A. and Rex, D.C. (1980): The evolution of excess argon in Alpine biotites – a $^{40}Ar/^{39}Ar$ analysis. *Earth Planet. Sci. Lett.* **48**, 185–208.

Royden, L.H. (1993): The tectonic expression of slab pull at continental convergent margins. *Tectonics* **12**, 303–325.

Samson, S.D. and Alexander, E.C., Jr. (1987): Calibration of the interlaboratory $^{40}Ar/^{39}Ar$ dating standard, Mmhb 1. *Chem. Geol. (Isotope Geosci. Sect.)* **66**, 27–34.

Schulmann, K., Ledru, P., Autran, A., Melka, R., Lardeaux, J.M., Urban, M. and Lobkowicz, M. (1991): Evolution of nappes in the eastern margin of the Bohemian Massif: a kinematic interpretation. *Geol. Rundsch.* **80**, 73–92.

Shand, P., Gaskarth, J.W., Thirlwall, M.F. and Rock, N.M.S. (1994): Late Caledonian lamprophyre dyke swarms of South-Eastern Scotland. *Mineral. Petrol.* **51**, 277–298.

Sparks, S.J. (1992): Magma generation in the earth. In: Brown, G.C., Hawkesworth, C.J. and Wilson, R.C.L. (eds.): Understanding the Earth. Cambridge University Press, Cambridge, pp. 91–114.

Steiger, R.H. and Jäger, E. (1977): Subcommission on geochronology convention on the use of decay constants in geo- and cosmochronology. *Earth Planet. Sci. Lett.* **36**, 359–362.

Stipska, P. and Schulmann, K. (1995): Inverted metamorphic zonation in a basement-derived nappe sequence, eastern margin of the Bohemian Massif. *Geol. J.* **30**, 385–413.

Streckeisen, A. (1979): Classification and nomenclature of volcanic rocks, lamprophyres, carbonatites and melilitic rocks. *N. Jahrb. Mineral. Abhandl.* **134**, 1–14.

Sun, S.S. (1982): Chemical composition and origin of Earth's primitive mantle. *Geochim. Cosmochim. Acta* **46**, 179–192.

Suppe, J. (1985): Principles of structural geology. Prentice Hall, Englewood Cliffs, 537 pp.

Tollmann, A. (1982): Großräumiger variszischer Deckenbau im Moldanubikum und neue Gedanken zum Variszikum Europas. *Geotekt. Forsch.* **64**, 1–91.

Turner, S., Arnaud, N., Liu, J., Rogers, N., Hawkesworth, C., Harris, N., Kelley, S., van Calsteren, P. and Deng, W. (1996): Post-collision, shoshonitic volcanism on the Tibetan plateau: Implications for convective thinning of the lithosphere and the source of ocean island basalts. *J. Petrol.* **37**, 45–71.

Turpin, L., Velde, D. and Pinte, G. (1988): Geochemical comparison between minettes and kersantites from the Western European Hercynian orogen: trace element and Pb–Sr–Nd isotope constraints on their origin. *Earth Planet. Sci. Lett.* **87**, 73–86.

Voggenreiter, W., Hötzl, H. and Mechie, J. (1988): Low-angle detachment origin of the Red Sea Rift system. *Tectonophysics* **150**, 51–75.

Vrána, S., Blümel, P. and Petrakakis, K. (1995): Moldanubian Zone – Metamorphic evolution. In: Dallmeyer, R.D., Franke, W. and Weber, K. (eds.): Pre-Permian Geology of Central and Eastern Europe. Springer-Verlag, Berlin- Heidelberg, pp. 453–466.

Waldmann, L. (1951): Das außeralpine Grundgebirge Österreichs. In: Schaffer, F.X. (ed.): Geologie von Österreich. 2. Ed., Deuticke, Wien, pp. 1–105.

Weber, K. and Duyster, J. (1990): Moldanubian Zone of the Waldviertel, Lower Austria. In: Franke, W. (ed.): Bohemian Massif. Field Guide, Conf. IGCP no. 233 "Paleozoic orogens in central Europe", Göttingen-Gießen, pp. 87–96.

Wendt, J.I., Kröner, A., Fiala, J. and Todt, W. (1994): U–Pb zircon and Sm–Nd dating of Moldanubian HP/HT granulites from South Bohemia, Czech Republic. *J. Geol. Soc. London* **151**, 83–90.

Wernicke, B. (1985): Uniform-sense normal simple shear of the continental lithosphere. *Canad. J. Earth Sci.* **88**, 108–125.

Wilson, M. (1991): Igneous Petrogenesis – a global approach. 2 Ed., HarperCollins Academic, London, 466 pp.

York, D. (1969): Least squares fitting of a straight line with correlated errors. *Earth Planet. Sci. Lett.* **5**, 320–324.

Received 23 January 2002, resubmitted 25 January 2004
Accepted in revised form 25 February 2004
Editorial handling: U. Schaltegger